GPF Deformable Model based Vessel Segmentation in CT

Si Yong Yeo[1]
genyeoius@gmail.com
Xianghua Xie[2]
x.xie@swansea.ac.uk
Igor Sazonov[1]
i.sazonov@swansea.ac.uk
Perumal Nithiarasu[1]
p.nithiarasu@swansea.ac.uk

[1] College of Engineering
Swansea University
Swansea, SA2 8PP, UK

[2] Department of Computer Science
Swansea University
Swansea, SA2 8PP, UK

Abstract

In this work, we present a method to segment carotid vessels from CT scans. Image denoising is performed using vessel enhancing diffusion, which can smooth out image noise and enhance vessel structures. The Canny edge detection technique which produces object edges with single pixel width is used for accurate detection of the lumen boundaries. The image gradients are then used to compute the geometric potential field which gives a global representation of the geometric configuration. The deformable model uses a regional constraint to suppress calcified regions for accurate segmentation of the vessel geometries. The preliminary result shows the prosed method achieves promising results based on qualitative evaluation using manual labelled groundtruth.

1 Introduction

The human circulatory system consists of vessels that transport blood throughout the body, providing the tissues with oxygen and nutrients. It is known that vascular diseases such as stenosis and aneurysms are often associated with changes in blood flow patterns and the distribution of wall shear stress. Modelling and analysis of the hemodynamics in the human vascular system can improve our understanding of vascular disease, and provide valuable insights which can help in the development of efficient treatment methods. One of the main challenges is the accurate reconstruction of the vascular geometry. The anatomical information used to reconstruct the geometric models are usually provided in the form of medical image datasets (scans) from imaging modalities such as computed tomography (CT) and magnetic resonance (MR) imaging. Manual reconstruction of the vasculature geometries can be tedious and time consuming. There is also the issue of variability between the geometries extracted manually by different individuals, and variability of geometries extracted by the same individual at different occasions.

Although several techniques exist for the segmentation of vascular structures from medical images, it remains an intricate process due to factors such as image noise, partial volume

effects, image artifacts, intensity inhomogeneity and changes in topology. In [11], the coordinate points for the center line of the aortic arch were extracted from volume rendered MR images. A cubic spline was then used to represent the aortic centerline, and cross-sectional grids were generated on normal planes at equidistant points along the curve. This generated a curved tube with circular cross section of uniform radius, which is not representative of the geometry of the aorta. In [15], the centerline and diameter information of the vessels was extracted from the image dataset, and the vascular model was reconstructed using non-uniform rational B-splines (NURBS). Such techniques may often smooth out geometric information that can be important to the computation of accurate flow dynamics, such as those at bifurcations.

The 3D models of the vascular structures are commonly reconstructed by extracting the 2D contours of the vessels at each of the image slices, and then lofting through the contours to create the surface models of the vessels, e.g. [3, 16, 19]. In [8, 9], a 3D dynamic surface model was used to delineate the boundary of carotid arteries. An initial triangulated model was placed within the interior of the carotid vessels, and an inflation force was applied to deform the model towards the vessel wall. In particular, the inflation force is applied only when the vertices of the model are within the lumen, i.e., at locations with image intensity below a user-specified threshold. An image-based force is further applied to the surface model to better localize the boundary. It may however be difficult to select an appropriate threshold value that delineates the vessel wall closely due to inhomogeneous image intensity. This approach is sensitive to noise, and manual editing is often required to move the vertices towards the vessel wall. In [13], a 2D discrete dynamic contour was first used to extract the vessel contours, a dynamic surface model was then inflated to reconstruct the surface model using the binary images of the extracted contours. This however does not consider the 3D geometric information from the image dataset. In [4, 5, 18], the surface models for each of the vessel branches of the carotid artery were reconstructed independently using a tubular deformable model. A surface merging algorithm is then required to reconstruct the surface model of the carotid bifurcation from the triangulated surfaces of the vessel branches. This particular approach requires the determination of the axis of each of the vessels, which can be done manually by selecting a reasonable amount of points from image slices to represent the curves of the structure. Due to the smoothing effect of this technique, regions of high curvature such as those at bifurcations or stenosis may not be modeled accurately. These explicit deformable models represent contours and surfaces parametrically, which requires the tracking of points on the curves and surfaces during deformation. It is therefore difficult for explicit deformable models to deal with topological variation and complex shapes.

Implicit deformable models have been applied in the segmentation of vascular structures in [1, 2, 6, 12, 14]. However, many of these techniques use an attraction force field which acts on contours or surfaces only when they are close to the object boundaries. As such, initial contours have to be placed close to the object boundaries, which can be tedious in complex geometries. A constant pressure term such as the one in [10], is often used to monotically expand or shrink the deformable model towards the image object boundaries, which can overwhelm weak object edges. In addition, the initial contours have to be placed either inside or outside object boundaries, which can be difficult for compact and narrow structures. Many of these techniques are also sensitive to image noise, and have difficulties in extracting deep boundary concavities.

2 Proposed Method

We propose a 3D deformable model based segmentation method to extract the carotid structures. The carotid vessels are first enhanced by applying anisotropic diffusion, and then vessel edges are localised using Canny edge detection which provides better edge localisation and connectivity compared to other conventional techniques, such as Sobel. The images gradient vectors at those edge locations identified by Canny edge detector are then used to compute a geometric potential field which gives a global representation of the geometric configuration. This field is then used to drive a 3D deformable model, with an additional simplistic regional constraint to suppress the interference from vessel calcificcation.

2.1 Vessel enhancing and edge detection

The formulation of the vessel enhancing diffusion filter is based on a smoothed version of the vesselness measure used in [7]. In this approach, an anisotropic diffusion filter with strength and direction determined by the vesselness measure is applied to enhance the geometric structures of the vessel. The vesselness measure is determined by analyzing the eigensystem of the Hessian matrix given as:

$$\mathbf{H} = \begin{bmatrix} I_{xx} & I_{xy} & I_{xz} \\ I_{yx} & I_{yy} & I_{yz} \\ I_{zx} & I_{zy} & I_{zz} \end{bmatrix} \tag{1}$$

which describes the geometric information at each point of a 3D image I based on the local intensity variations. Here, the derivatives of the image I are computed as convolution with derivatives of the Gaussian function, i.e. $I_x = I(\mathbf{x}) * \frac{\partial}{\partial x} G_\sigma(\mathbf{x})$, where G_σ denotes the Gaussian function with standard deviation σ. The principal curvatures and directions are given by the maximum and minimum eigenvalues and the corresponding eigenvectors. With the eigenvalues given such that $|\lambda_1| \leq |\lambda_2| \leq |\lambda_3|$, the vesselness measure is defined as: if $\lambda_2 \geq 0$ or $\lambda_3 \geq 0$, $V_\sigma(\lambda) = 0$; otherwise $V_\sigma(\lambda) = \left(1 - e^{\frac{-{R_A}^2}{2\alpha^2}}\right) \cdot e^{\frac{-{R_B}^2}{2\beta^2}} \cdot \left(1 - e^{\frac{-S^2}{2\gamma^2}}\right) \cdot e^{\frac{2c^2}{|\lambda_2|{\lambda_3}^2}}$ with $R_A = \frac{|\lambda_2|}{|\lambda_3|} R_B = \frac{|\lambda_1|}{\sqrt{|\lambda_2 \lambda_3|}} S = \sqrt{{\lambda_1}^2 + {\lambda_2}^2 + {\lambda_3}^2}$in which R_A and R_B can be used to differentiate tubular structures from blob-like and plate-like structures, while S is used to differentiate between foreground vessel structures and background noise. The parameters α, β and γ are weighting factors which control the sensitivity of the vesselness measure, and c is a small constant.

For a multiscale analysis, the vesselness function is computed for a range of scales, and the maximum response is selected using the following equation: $V = \max_{\sigma_{min} \leq \sigma \leq \sigma_{max}} V_\sigma(\lambda)$A diffusion tensor is then defined such that vessel diffusion takes place in the direction of the vessel, while diffusion perpendicular to the vessel direction is inhibited. The diffusion tensor can therefore be used to preserve vessel structures and is given as: $\mathbf{D} = \mathbf{Q}\lambda'\mathbf{Q}^T$ where $\mathbf{Q}$ is a matrix containing the eigenvectors of the Hessian matrix $\mathbf{H}$, and λ' is a diagonal matrix with elements given as: ${\lambda_1}' = 1 + (w-1) \cdot V^{\frac{1}{s}}$, ${\lambda_2}' = {\lambda_3}' = 1 + (\varepsilon - 1) \cdot V^{\frac{1}{s}}$ with w, ε and s as tuning parameters. The anisotropic diffusion is then defined as: $L_t = \nabla \cdot (\mathbf{D} \nabla L)$where $L(0)$ is set as the input image.

The Canny edge detection can produce object edges with single pixel width, and can therefore be used for more accurate edge detection of the vessel structures. The image gra-

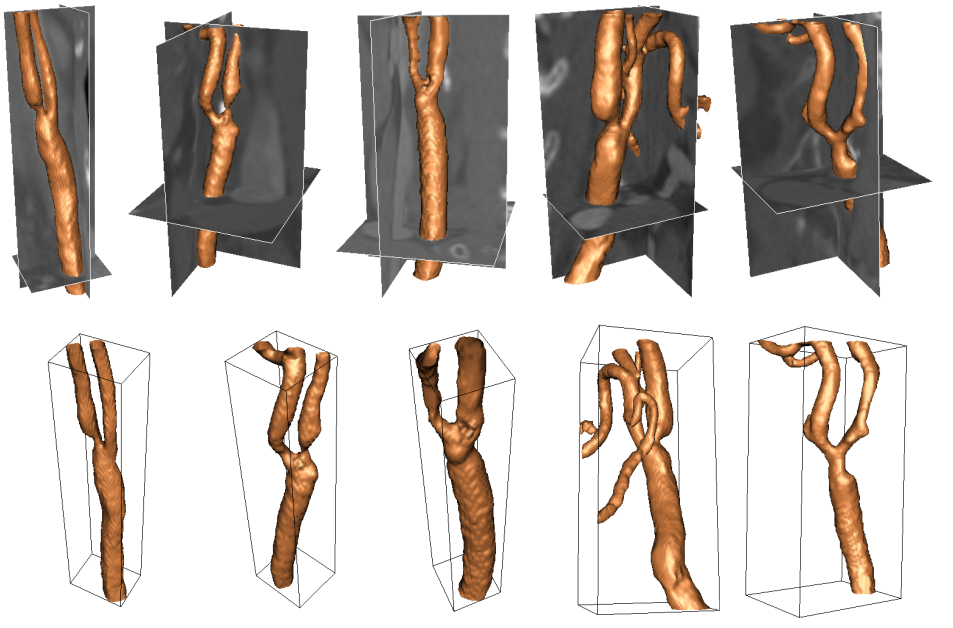

Figure 1: Segmentation of carotid artery from CT image dataset.

dients at the detected edges are then used to compute the geometric potential field, which is briefly described in the following section.

2.2 GPF based segmentation with a simplistic region constraint

It is shown in [17] that the GPF deformable model can be used to efficiently segment complex geometries from biomedical images. By using pixel or voxel interactions across the whole image domain, the deformable model is more robust to image noise and weak edges. The dynamic vector force field changes according to the relative postition and orientation between the geometries, which allows the deformable model to propagate through long tubular structures. Here, the GPF deformable model is applied to segment the geometries of human carotid arteries from CT images. Some of the main challenges in the segmentation of the carotid geometries include intensity inhomgeneity, weak edges and adjacent veins with similar intensities to the carotids. In addition, calcifications which are attached to the arterial walls should not be included in the reconstructed geometries. Although, the calcified plaques often appear as relatively bright regions compared to soft tissues, plaques with lower densities may have similar intensities to the lumen. As the intensities of the plaques vary with the densities, it is not easy for techniques such as global intensity threshold to remove the plaques from the extracted geometries. In this section, a simple heuristic region constraint is added to the deformable model such that it does not propagate across the calcified regions. This is done by constraining the deformable model from propagating across regions with image gradient magnitude larger than a user specified value, T_{max}. As the calcified regions usually have relatively large image gradients, the threshold value can be easily selected by observing the histogram of the image gradient magnitude. The deformable model with

region constraint can thus be expressed as:

$$\frac{\partial \phi}{\partial t} = \begin{cases} 0 & \text{if } |\nabla I| > T_{max} \\ \alpha g \kappa |\nabla \phi| - (1-\alpha)(\mathbf{F} \cdot \nabla \phi) & \text{otherwise} \end{cases} \quad (2)$$

where α is a weighting parameter, g is the edge stopping function, κ is the curvature and $\mathbf{F}$ is the geometric potential force defined in the GPF model [17].

3 Results

In this section, experimental results on the segmentation of the cartoid geometries using the proposed framework are shown. Six datasets from CT imaging are used in the experiment. The volumes of interest containing the carotid arteries are extracted from the image datasets to reduce the size of the input datasets.

Figure 1 shows the segmentation of the carotid geometries using the GPF deformable model with region constraint. The bidirectional and dynamic vector force allows the flexible cross-boundary intializations of the model to easily propagate and converge to the geometries of the carotid arteries. Note that the deformable model easily propagate through the stenotic carotid bifurcations and get around the calcified regions to efficiently segment the carotid geometries from the CT images.

The reconstructed vessel geometries using the proposed method are compared against geometries from manual segmentation. Figure 2 demonstrates the comparison of the extracted geometries using random cross-section slices taken along the z-axis direction. The blue and orange contours represent the cross-section of the geometries extracted manually and using the GPF deformable model respectively. As shown in the figures, the image dataset consist of other tissue structures which may affect the geometric reconstruction. In particular, vessels adjacent to the carotid artery can often cause other models to leak out due to the similar intensity. The geometric potential field provides a more coherent and global representation of the object edges, and allows the deformable model to extract the geometry accurately. By adding a region constraint, the proposed model can reasonably cope with the calcified regions as the deformable model propagates through the tubular structures to segment the vessel geometry. Quantitative analysis based on manual labelling showed promising result. The average foreground accuracy, background accuracy and overall accuracy are 93.9%, 99.8% and 96.8%, respectively. Note, these are normalised accuracy measurement to reduce measurement bias towards the large number of background voxels in the image.

References

[1] L. Antiga and A. Ene-Iordache, B. Remuzzi. Computational geometry for patient-specific reconstruction and meshing of blood vessels from mr and ct angiography. *IEEE T-MI*, 22(5):674–684, 2003.

[2] L. Antiga, M. Piccinelli, L. Botti, B. Ene-Iordache, A. Remuzzi, and Steinman D. A. An image-based modeling framework for patient-specific computational hemodynamics. *Medical and Biological Engineering and Computing*, 46(11):1097–1112, 2008.

[3] A. D. Augst, D. C. Barratt, A. D. Hughes, S. A. McG Thom, and X. Y. Xy. Various issues relating to computational fluid dynamics simulations of carotid bifurcation flow based on models reconstructed from three-dimensional ultrasound images. *Proc Inst Mech Eng H, Journal of Engineering in Medicine*, 217(5):393–403, 2003.

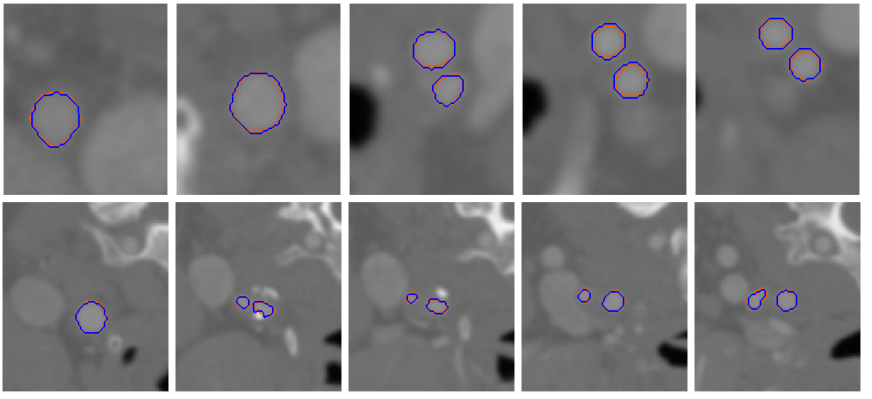

Figure 2: Comparison of geometry segmented from CT image dataset 1 using image slices taken along z-axis direction: blue - manual, orange - GPF deformable model.

[4] J. R. Cebral, R. Lohner, O. Soto, P. L. Choyke, and P. J. Yim. Patient-specific simulation of carotid artery stenting using computational fluid dynamics. In *MICCAI*, pages 153–160, 2001.

[5] J. R. Cebral, M. A. Castro, R. Lohner, J. E. Burgess, R. Pergolizzi, and C. M. Putman. Recent developments in patient-specific image-based modeling of hemodynamics. In *ENIEF04*, 2004.

[6] T. Deschamps, P. Schwartz, D. Trebotich, P. Colella, D. Saloner, and R. Malladi. Vessel segmentation and blood flow simulation using level-sets and embedded boundary methods. In *Computer Assisted Radiology and Surgery*, pages 75–80, 2004.

[7] A. F. Frangi, W. J. Niessen, K. L. Vincken, and M. A. Viergever. Multiscale vessel enhancement filtering. In *MICCAI*, pages 130–137, 1998.

[8] J. D. Gil, H. M. Ladak, D. A. Steinman, and A. Frenster. Accuracy and variability assessment of a semiautomatic technique for segmentation of the carotid arteries from three-dimensional ultrasound images. *Medical Physics*, 27(6):1333–1342, 2000.

[9] H. M. Ladak, J. S. Milner, and D. A. Steinman. Rapid three-dimensional segmentation of the carotid bifurcation from serial MR images. *Journal of Biomechanical Engineering*, 122(1):96–99, 2000.

[10] R. Malladi, J. A. Sethian, and B. C. Vemuri. Shape modelling with front propagation: A level set approach. *IEEE T-PAMI*, 17(2):158–175, 1995.

[11] D. Mori and T. Yamaguchi. Construction of the CFD model of the aortic arch based on mr images and simulation of the blood flow. In *International Workshop on Medical Imaging and Augmented Reality*, pages 111–116, 2001.

[12] B. Nilsson and A. Heyden. A fast algorithm for level set-like active contours. *Pattern Recognition Letters*, 24(9):1311–1337, 2003.

[13] D. A. Steinman, J. B. Thomas, H. M. Ladak, J. S. Milner, B. K. Rutt, and J. D. Spence. Reconstruction of carotid bifurcation hemodynamics and wall thickness using computational fluid dynamics and mri. *Magnetic Resonance in Medicine*, 47(1):149–159, 2002.

[14] J. Svensson, R. Gardhagen, E. Heiberg, T. Ebbers, D. Loyd, T. Lanne, and M. Karlsson. Feasibility of patient specific aortic blood flow CFD simulation. In *MICCAI*, pages 257–263, 2006.

[15] Y. Tokuda, M.-H. Song, Y. Ueda, A. Usui, A. Toshiaki, S. Yoneyama, and S. Maruyama. Three-dimensional numerical simulation of blood flow in the aortic arch during cardiopulmonary bypass. *European Journal of Cardio-thoracic Surgery*, 33(2):164–167, 2008.

[16] X. Y. Xu, Q. Long, M. W. Collins, M. Bourne, and T. M. Griffith. Reconstruction of blood flow patterns in human arteries. *Proc Inst Mech Eng H, Journal of Engineering in Medicine*, 213(5): 411–421, 1999.

[17] S. Y. Yeo, X. Xie, I. Sazonov, and P. Nithiarasu. Geometrically induced force interaction for three-dimensional deformable models. *IEEE T-IP*, 20(5):1373–1387, 2011.

[18] P. J. Yim, J. J. Cebral, R. Mullick, H. B. Marcos, and R. L. Choyke. Vessel surface reconstruction with a tubular deformable model. *IEEE T-MI*, 20(12):1411–1421, 2001.

[19] H. F. Younis, M. R. Kaazempur-Mofrad, R. C. Chan, A. G. Isasi, D. P. Hinton, A. H. Chau, L. A. Kim, and R. D. Kamm. Hemodynamics and wall mechanics in human carotid bifurcation and its consequences for atherogenesis: investigation of inter-individual variation. *Biomechanics and Modeling in Mechanobiology*, 3(1):17–32, 2004.